Latin American Journal of Energy Research - Lajer
periodicos.ufes.br/lajer

Latin American Journal of Energy Research – Lajer (2024) v. 11, n. 1, pp. 12–23
https://doi.org/10.21712/lajer.2024.v11.n1.p12-23

Development of the Rodsim numerical simulator for the study of a sucker rod pump, comparing the Gibbs (1963) and Lea (1990) models

Fernando Cyrilo de Oliveira[1], Oldrich Joel Romero[2,*]

[1] Engenheiro de Operações, Halliburton, Macaé, RJ, Brasil
[2] Professor, Federal University of Espírito Santo – Ufes, Sao Mateus, ES, Brasil
*Corresponding author, E-mail: oldrich.romero@ufes.br

Received: 31 January 2024 | Accepted: 31 May 2024 | Published online: 5 June 2024

Abstract: It is of great importance to be fully cognizant of the sucker rod pump system in order to make reliable production forecasts and to evaluate potential strategies for optimizing production processes. A frequently employed methodology in such circumstances is numerical simulation. A numerical sucker rod pump simulator can provide valuable insights into production performance by generating dynamometric charts that represent the efficiency of this activity. Since the rod column behaves like a thin rod, it is possible to represent the mathematical model by a one-dimensional wave equation that describes the forces acting on this rod column. Lea (1990), proposing an improvement of the work of Gibbs (1963), considers the effects of the viscosity of the fluid produced in a vertical well without heat exchange, the piston diameter, the production column and the rods to obtain the damping factor, thus being more complete and producing a more accurate result in the dynamometric charts. Both models are implemented and discussed herein. The equations are discretized and solved in the Matlab® environment. The code includes a graphical user interface that generates the internal Rodsim application. The application is used to solve a typical case of a sucker rod pump and to obtain the surface and downhole dynamometric plots for certain scenarios.
Keywords: Sucker rod pump. Rod Column. Dynamometric chart. Numerical simulation.

1 Introduction

When oil flows to the surface due solely to the energy within the reservoir, it is said to be flowing naturally. However, the production by natural flow is a condition that normally occurs as soon as the productive life of the well begins. As the reservoir energy is depleted, or the production flow is reduced to uneconomical limits, additional energy is required to mobilize the bottom-to-surface fluids. In this manner, the production is accomplished through the use of artificial lift.

Among the available techniques for operating at the well domain, the sucker rod pump is one of the more frequently selected methods. As reported by Costa (2008), the sucker rod pump is utilized as a method for artificial lift in over 70% of oil wells globally.

The energy is transmitted to the fluid through an alternative pump positioned at the bottom of the well, which is driven by the pumping unit installed on the surface near the wellhead to transform the rotary motion into reciprocating motion. A column of rods serves to transmit the reciprocating motion to the pump, which is situated at the bottom of the well. The principal components of the sucker rod pump are the motor, rod column, subsurface pump, and tubing, as illustrated in Figure 1.

The pumping unit is typically connected to an electrical engine or an internal combustion engine via a gearbox that facilitates torque transmission, transforming the rotating movement of the engine into an alternate movement. The sucker rod, in turn, transmits the mechanical energy received at the surface to the subsurface. It should be noted that some energy is lost in the process due to friction (Souza, 2009; Rowlan, Mccoy and Podio, 2005; Silva et al., 2014).

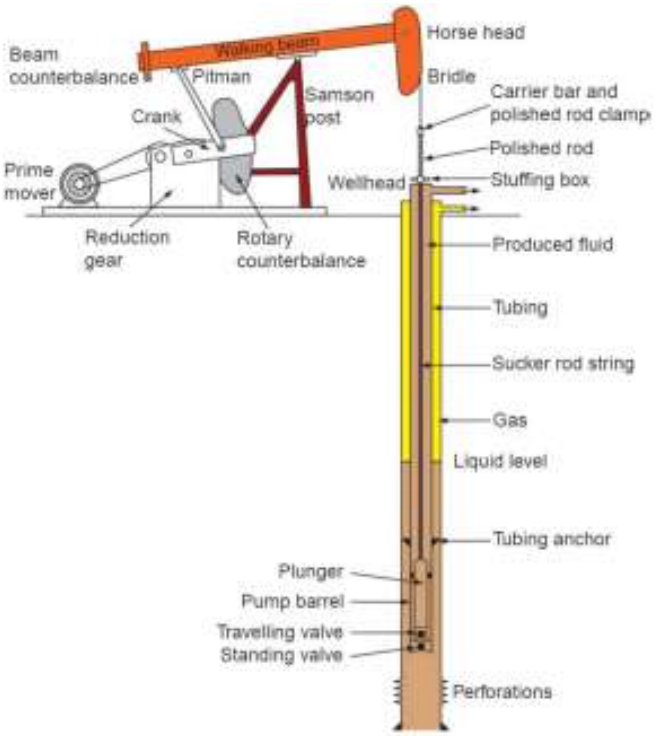

Figure 1. Typical configuration of a sucker rod pump. Source: Bellarby (2009).

One method for verifying the operational status of the system is to analyze surface dynamometer card (SDC) or downhole dynamometer card (DDC). The SDC is generated by recording a dynamometer that is coupled to the polished rod, the DDC is calculated from the SDC using a mathematical model. The DDC is also identified by dynagraph, or computer pump card, or bottomhole pump card.

In shallow wells or in wells operating at low pumping speed, interpretation on the SDC is relatively effective method in inferring bottomhole equipment performance.

In deeper wells or in well operating at high speeds, determination of downhole equipment performance form SDC is quite impossible. For this reason, the accurate generation of DDC is of great importance.

Two scientific contributions were very relevant for the study of the sucker rod pump through the dynamometric charts. The first one was given by Gibbs (1963) who simulated the dynamic behavior of the rod column by solving a damped wave equation. Later, Lea (1990) introduced the fluid flow model in the annulus, deriving an expression for the damping coefficient as a function of the piston, tubing and rods diameters and the viscosity of the fluid produced.

In this context, this work has developed a tool to simulate the behavior of a well equipped with a sucker rod pumping system based on Gibbs and Lea models.

This in-house software is a tool both for classroom use, to help transfer theoretical concepts to undergraduate and graduate students, and for field use, as the Federal University of Espírito Santo is located in an oil-producing region with new operators such as Seacrest Petroleo, Imetame Energia, EnP Energy Platform, and Mandacaru Energia.

2 Dynamometric chart

The downhole dynamometric chart is an important tool for analyzing and evaluating the condition of the downhole pump, since it shows the effects generated by the load on the downhole pump during a pumping cycle.

The load variation that occurs on a polished rod as it moves through the pumping cycle is registered by the surface dynamometer card (SDC). The forces acting on the polished rod at the top of the rod column during its movement are measured by a dynamometer installed between the clamp and the pumping unit table. As the forces generated by a downhole pump propagate through a rod column, these effects can be observed on the downhole dynamometer card (DDC). One factor that should be considered to be influential in this process is the elastic behaviour of the rod. Consequently, the SDC is unable to accurately reflect the actual behavior of the well pump. In order to obtain a DDC, it is necessary to utilise specialised tools at the bottom of the well or to employ mathematical models that utilise the SDC as a basis for obtaining a DDC.

Figure 2 depicts a theoretical dynamometric diagram. The horizontal axis represents the piston position, while the vertical axis depicts the piston load. The segments *c* and *e* represent the contraction and elongation of the rod and the production columns, respectively. The lines *Ftv* and *Fsv* represent the maximum and minimum loads, respectively. The aforementioned lines are drawn with the pump unit stopped near the endpoints of the upstroke (for *Ftv*) and the downstroke.

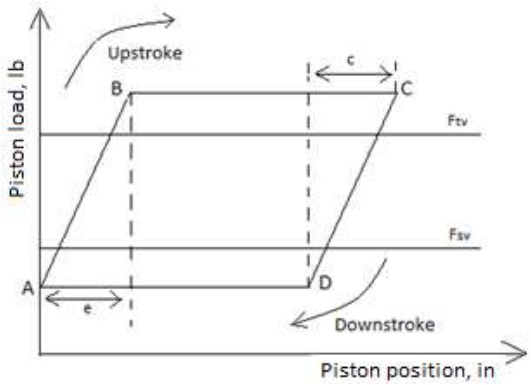

Figure 2. Theoretical downhole dynamometric chart (Gomes, 2009).

Point A represents the commencement of the upstroke, during which the travelling valve closes and the standing valve opens. At this point, the weight of the fluid column begins to be transferred to the rod column. This elongation will continue as the fluid column is lifted by the weight of the fluid column. At point B, the entire load of the fluid column is already acting on the rod column, which is already fully elongated. Consequently, the charges will remain constant until the point C, which represents the end of the upstroke and the beginning of the downstroke.

At point C, the standing valve closes, and the traveling valve opens. The weight of the fluid column is transferred from the rod column to the tubing to point D, where the entire weight of the fluid is acting on it. At point D, the end of the contraction of the rod column is observed, and the load remains constant until point A.

The dynamometric chart, as illustrated in Figure 3, can be utilized to identify potential issues during the mechanical pumping operation with rods.

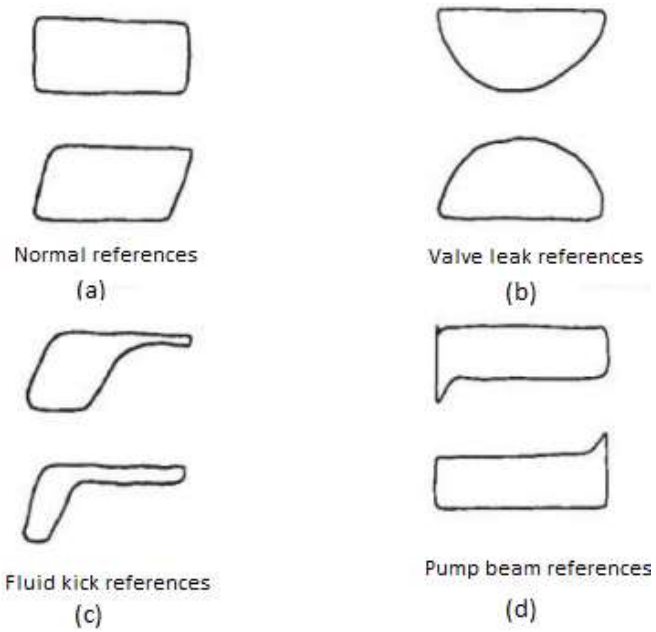

Figure 3. Typical downhole dynamometric charts (Lima et al., 2009).

The valve leak references charts (Figure 3b) indicate that when the rod is elevated, drawing fluid to the surface, the traveling valve fails, thereby demonstrating irregularity in the process. Consequently, the traveling valve does not seal, resulting in the column rising with production loss.

The chart with fluid kick references (Figure 3c) illustrates a pumping reading in which the well flow rate is less than the flow rate of the tubing can absorb. Consequently, the pump is frequently stopped in order to compensate for fluid loss and the associated cost of the process.

The pump beam references charts (Figure 3d) illustrates the fault that occurs automatically when the fluid level is in the pump. When the lifting capacity of the pump exceeds the feed rate of the reservoir, the pump is not completely filled. Consequently, at the beginning of the downward movement, the traveling valve does not open, and the piston remains with all the weight of the fluid above it. The piston encounters the fluid level at high speed, resulting in a substantial impact that is transmitted to the surface by the rod column. This scenario is suboptimal and can potentially lead to several structural damages to the system (Lima et al., 2009).

When the DDC plot displays a rectangle, it signifies optimal pumping conditions. These conditions are characterized by a rigid and inelastic rod, a low pumping speed (eliminating dynamic forces), an incompressible fluid, and an anchored rod tube. Any energy losses along the rod are to be avoided (Guo et al., 2007).

The study of the behavior of the rod column and thus of the subsurface pump is of significant importance, as its behavior directly influences the overall efficiency of the system. The primary objective of the sucker rod pump is to extract the maximum amount of oil. If this system is not functioning properly, the extracted volume will be smaller than expected.

This research presents a simulator of an artificial elevation system equipped with a sucker rod pump, which is based on the solution of the wave equation for a vertical well without heat exchange, considering the viscosity of the fluid and elongation effects of the rod. The surface and downhole dynamometric charts are the main focus of this study.

The solution of the governing equations, with appropriate initial boundary conditions, is obtained using the so-called finite difference method. The computational code is implemented using the MathWorks MATLAB® software.

3 Mathematical model: wave equation

The geometry adopted (Figure 4) is represented by a vertical column of length L and diameter d. This column is located within a vertical well that is not shown in the figure. Points A and B, respectively, represent the moorings with the polished rod and the bottom pump (in the subsurface). In these points, the boundary conditions, A - kinematics of the pump unit and B - operation of the bottom pump, are applied to the solution of the valid equation in the internal points.

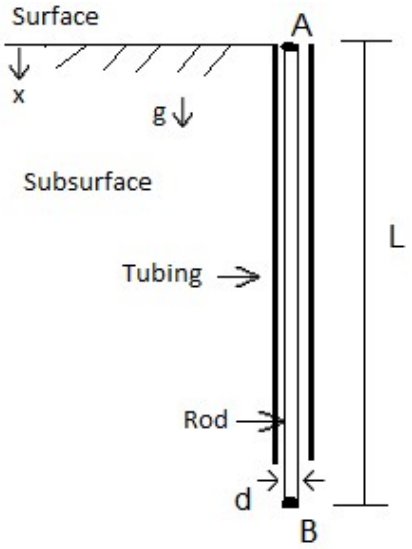

Figure 4. Schematic representation of the geometry adopted (figure not in scale).

The wave equation is defined by an analysis of the forces acting on the rod column. Figure 5 illustrates these driving forces. The element is defined by a cross-sectional area A, a time t, the variable x, which represents any point in the rod column, and Δx, which is the displacement from that point.

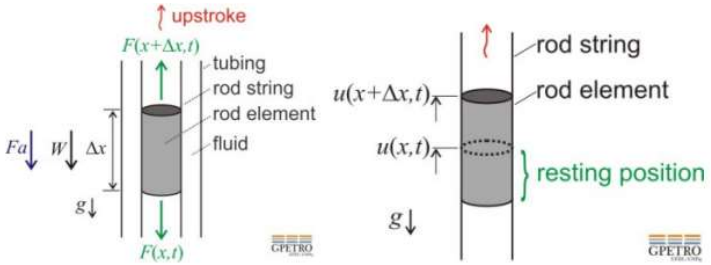

Figure 5. Outline of the directions of the forces acting on a rod differential element (Romero and Almeida, 2014).

Additionally, Figure 5 illustrates that $T(x,t)$ and $T(x+\Delta x,t)$ represent the tensile forces exerted by the sections above and below the element, respectively. Furthermore, *W* represents the weight of the rod element, while *Fa* denotes the damping force acting to oppose the movement of the rods. The remaining variables, *g* and *v*, respectively denote gravitational force and velocity.

Newton's second law states that the ratio of linear momentum, defined as the product of mass (*m*) and velocity (*v*) of the differential element and time (*t*), is equal to the sum of forces acting on the element. This can be expressed as $\frac{\mathrm{d}(mv)}{\mathrm{d}t} = \sum F$.

It is important to note that, despite the elongated nature of the element, the mass (*m*) remains constant, given that the area (*A*) and the distance between the two points (Δx) are also constant. Consequently, the weight of the density element ρ is given by $W = mg$. Utilizing the aforementioned information and the variables presented in Figure 5, we can derive the following equation $\frac{d(\rho A\Delta x v)}{dt} = T(x+\Delta x,t) - T(x,t) + \rho A\Delta x g + F_a\Delta x$. Dividing by Δx and considering the limit $\Delta x \to 0$, the previous equation is written as $\frac{d(\rho A v)}{dt} = \frac{d(T)}{dt} + A\rho g + F_a$. Whereas the term F_a is approximated by the product of velocity *v* with the constant *k*, $F_a = -kv$. The tension is obtained from Hooke's Law $T = EA\frac{[u(x+\Delta x,t)-u(x,t)]}{\Delta x}$, where *E* is the modulus of elasticity.

In the limit $\Delta x \to 0$, the Hooke equation can be rewritten as $T = EA\frac{du}{dx}$, and from $v = \frac{d(x+u(x,t))}{dx} = \frac{du(x,t)}{dx}$, it follows that the one-dimensional partial transient differential equation, which has been renamed the one-dimensional viscous friction wave equation, can be derived:

$$\frac{d^2u(x,t)}{dt^2} = \frac{E}{\rho}\frac{d^2u(x,t)}{dx^2} - \frac{k}{A\rho}\frac{du(x,t)}{dt} + g, \tag{1}$$

or, in accordance with the definition provided by Gibbs (1963)

$$\frac{d^2u(x,t)}{dt^2} = a^2\frac{d^2u(x,t)}{dx^2} - \varsigma\frac{du(x,t)}{dt} + g, \tag{2}$$

where $a = \sqrt{E/\rho}$ is the propagation velocity of the wave in the rod.

In 1990, Lea extended the work of Gibbs (1963) by deriving an expression for the damping coefficient as a function of the fluid viscosity (η) produced, the piston diameter, the tubing diameter, and the rod diameter. Lea (1990) considers that the piston and rod column velocities (v_r) were approximately equal, and that the annular flow was Newtonian, laminar, incompressible, single-phase, and fully developed fluid flow. Consequently, the damping coefficient (ς) was expressed by Eqs. (3) and (4).

$$\varsigma = \frac{2\pi r_r \eta}{\rho_r A_r}\left(K_1 + K_2\frac{A_r}{A_t - A_r}\right), \text{if } v_r < 0, \tag{3}$$

$$\varsigma = \frac{2\pi r_r \eta}{\rho_r A_r}\left(K_1 - K_2\frac{A_p - A_r}{A_t - A_r}\right), \text{if } v_r > 0, \tag{4}$$

where, A_t represents the cross-sectional area of the tubing, A_r the cross−sectional area of the rod, A_p the cross-sectional area of the piston, ρ_r the specific mass of the rod material and K_1 and K_2 are geometric factors as a function of the diameters of the tubing and the rods, as shown in Eqs. (5) and (6).

$$K_1 = \frac{(r_t{}^4 - r_r{}^4)ln\frac{r_r}{r_t} + (r_t{}^2 - r_r{}^2) - [2r_r{}^2 \ln\left(\frac{r_r}{r_t}\right) + (r_t{}^2 - r_r{}^2)]^2}{r_r ln\frac{r_r}{r_t}[(r_t{}^4 - r_r{}^4)ln\frac{r_r}{r_t} + (r_t{}^2 - r_r{}^2)^2]}, \quad (5)$$

$$K_2 = \frac{2(r_t{}^2 - r_r{}^2)[2r_r{}^2 \ln\left(\frac{r_r}{r_t}\right) + (r_t{}^2 - r_r{}^2)]}{r_r[(r_t{}^4 - r_r{}^4)ln\frac{r_r}{r_t} + (r_t{}^2 - r_r{}^2)^2]}, \quad (6)$$

r_t is the radius of the tubing.

By solving the wave equation, Eq. (2), it is possible to obtain the unknowns $u(x_i, t_{j+1})$ and thus, draw the dynamometric charts through the simulator.

3.1 Initial conditions

A number of hypotheses were employed in the construction of the geometry, which comprises a column of vertical rods (without gloves and without centralizers) of length *L* and diameter *d* that is constant, without gas interference, constant angular velocity of the counterweights, pump filled by the fluid, and the inertia of the fluid is disregarded.

As a preliminary assumption for the calculations, at a time $t = 0$, the system can be considered at rest and can be mathematically represented by Eqs. (7) and (8).

$$u(x, 0) = 0, \quad (7)$$

$$\frac{du(x,0)}{dt} = 0. \quad (8)$$

Boundary conditions are employed within the limits of the rod column: at the surface, through the position of the polished rod, and in subsurface, through the operating condition of the pump. According to According to Tákacs (2002), the most used approach to describe the movement of the polished bar is a harmonic movement. Eq. (9) indicates the polished rod position $s(\theta)$ on the surface according of the crank angle θ, the stroke of the polished rod is indicated by *S*.

Boundary conditions are employed within the limits of the rod column. At the surface, this is achieved through the position of the polished rod. In the subsurface, it is accomplished through the operating condition of the pump.

In accordance with Tákacs (2002), the most prevalent methodology for characterizing the motion of the polished bar is a harmonic approach. Eq. (9) illustrates the relationship between the polished rod position, $s(\theta)$, on the surface and the crank angle, θ, as well as the stroke of the polished rod, *S*.

$$s(\theta) = \frac{S}{2}(1 - cos\theta), \quad (9)$$

As stated by Tákacs (2002), the effective piston stroke (S_p) is influenced by the elongation of the production column (e_t) and the rod column (e_r), which occurs due to fluid loading. Furthermore, Costa (1995) posits that the dynamic elongation (e_{ra}) also contributes to this discrepancy. Consequently, the piston stroke can be represented mathematically by Eq. (10).

$$S_p = S + e_{ra} - (e_t + e_r), \quad (10)$$

$$e_t = F_o E_t L, \quad (11)$$

$$e_r = F_o E_r L\,, \quad (12)$$

where, F_o is the fluid weight in the piston, E_t and E_r are the elastic constants of the materials of the production column and the rod column, respectively. The dynamic elongation (e_{ra}), as defined by Costa (1995), is expressed by Eq. (13).

$$e_{ra} = \frac{a_{max}\rho_r L}{E_r} \quad (13)$$

the maximum acceleration of the rods, a_{max}, is given by the expression $\frac{\omega^2 S}{2}$, where $\omega = 2\pi N$ is the angular velocity, and N is the pumping frequency. The specific mass of the rods, ρ_r, is also a factor in this equation.

4 Numerical solution of the wave equation

The rod column was divided into several discrete elements. Consequently, the governing equations for the deformation of the rod column were discretized by the finite difference method and explicit time-stepping technique.

The continuous differential equation, Eq. (2), is evaluated at discrete points (x_i, t_j) (Fig. 6), resulting in the following:

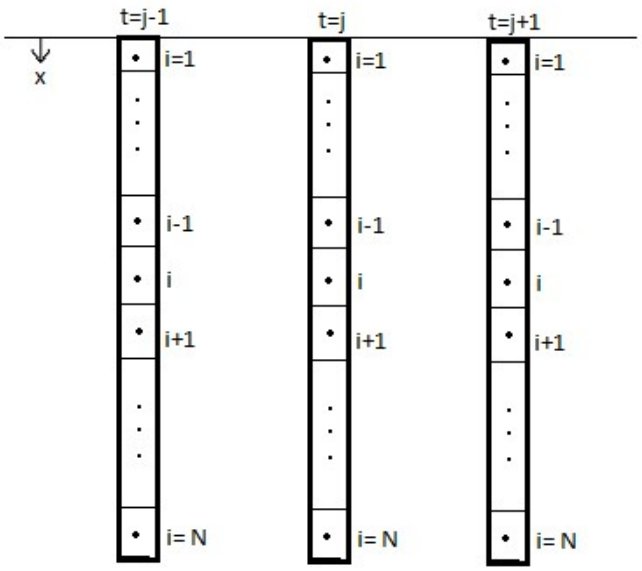

Figure 6. Schematic representation of the tubing to perform spatial and temporal discretization.

$$\frac{d^2u(x_i,t_j)}{dt^2} = a^2 \frac{d^2u(x_i,t_j)}{dx^2} - \varsigma \frac{du(x_i,t_j)}{dt} \tag{14}$$

All three terms of Eq. (14) are approximated by finite differences, expressed as follows:

$$\frac{u(x_i,t_{j+1})-2u(x_i,t_j)+u(x_i,t_{j-1})}{\Delta t^2} \approx a^2 \frac{u(x_{i+1},t_j)-2u(x_i,t_j)+u(x_{i-1},t_j)}{\Delta x^2} - \varsigma \frac{u(x_i,t_{j+1})-u(x_i,t_{j-1})}{2\Delta t}. \tag{15}$$

Eq. (15) is rewritten as follows:

$$u(x_i,t_{j+1}) \approx \frac{1}{\frac{\varsigma\Delta t}{2}+1}\{\left(\frac{a\Delta t}{\Delta x}\right)^2 u(x_{i+1},t_j) + [2 - 2\left(\frac{a\Delta t}{\Delta x}\right)^2]u(x_i,t_j) + \left(\frac{a\Delta t}{\Delta x}\right)^2 u(x_{i-1},t_j) + (\frac{\varsigma\Delta t}{2} - 1)u(x_i,t_{j-1})\} \tag{16}$$

The CFL (Courant, Friedrichs, and Lewy) condition is employed to obtain solutions for discrete equations of this nature. The dimensionless Courant number, denoted by *Co*, is defined as $Co = \frac{a\Delta t}{\Delta x}$, where a is the wave velocity, Δt is the interval, and Δx is the size of the mesh element. According to this condition, the Courant number must be less than or equal to one for the method to be developed (Thomas, 1995). Consequently, the Courant number is set to one in the present study, and Eq. (16) is simplified to:

$$u(x_i,t_{j+1}) \approx Au(x_{i+1},t_j) + Bu(x_{i-1},t_j) + Cu(x_i,t_{j-1}), \tag{17}$$

where *A*, *B* and *C* are constants expressed by

$$A = B = \frac{1}{\frac{\varsigma\Delta t}{2}+1} \; ; \; C = \frac{\frac{\varsigma\Delta t}{2}-1}{\frac{\varsigma\Delta t}{2}+1} \tag{18}$$

Is should be noted that Eqs. (17) and (18) provides a response as a function of three points (x_{i+1}, t_j) ,(x_{i-1}, t_j) e (x_i, t_{j-1}). For further details, please refers to Schmidt and Doty (1989) and Doty and Schmidt (1983).

5 The Rodsim academic simulator

The discrete equations, Eqs. (17) and (18), and boundary conditions were implemented in MathWorks MATLAB® software, as the environment allows an easy graphical visualization for the dynamometric charts and has ready-made libraries that facilitate the iterative calculation. A Graphical User Interface (GUI) was also developed resulting in the creation of our in-house simulator, RodSim (the formalization of the software's name is currently being processed).

In the simulator, users may select between the models of Gibbs (1963) and Lea (1990) and input several parameters, including the modulus of elasticity of the rod material, the speed of sound in the rods, the rod column length, the specific weight of rod material, the polished rod stroke, the pumping speed, the fluid's specific gravity, the tubing diameter, the piston diameter, the rod diameter, and the fluid's produced viscosity (Figure 7).

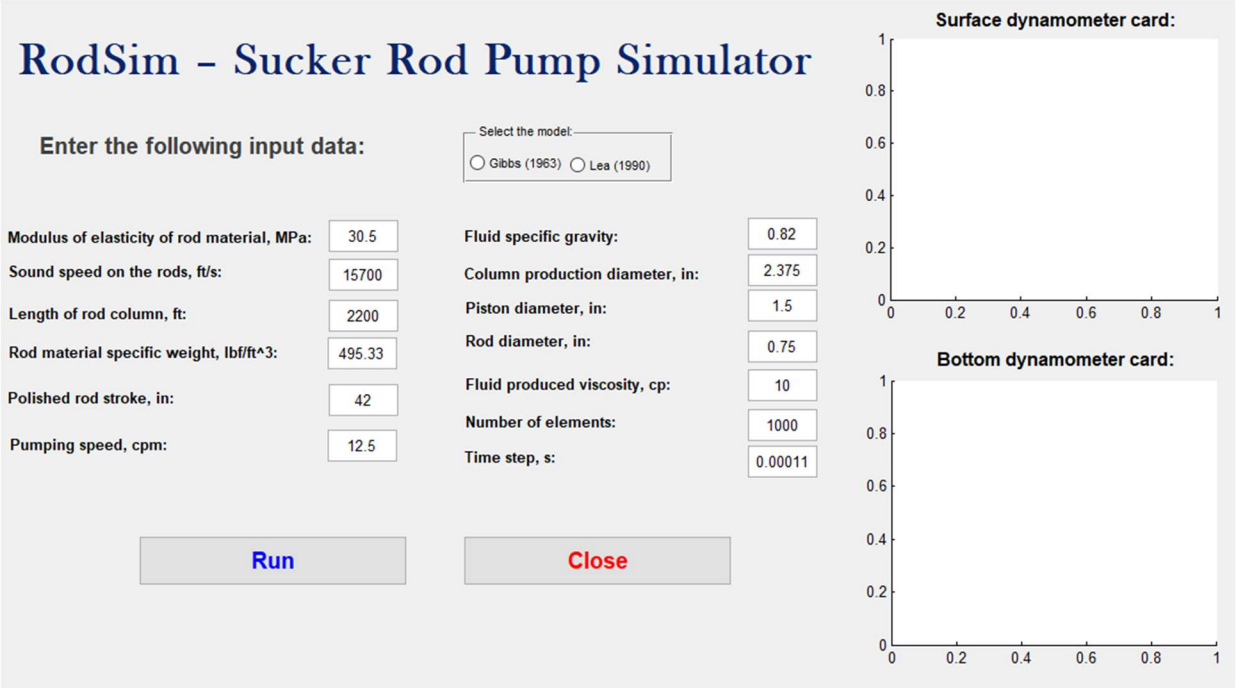

Figure 7. Layout of RodSim simulator.

Once the user has entered the desired values and selected the desired model type, the program will generate two dynamometric charts in the same window, as illustrated in Figure 7. These charts will be the surface dynamometric chart and the downhole dynamometric chart. This approach allows for the observation of the production process.

6 Rodsim application

The simulator permits the user to ascertain dynamometric charts according to the input data utilized. In this case study, the operational characteristics of the system are presented in Table 1. These data were derived from Romero and Almeida (2014).

The parameters for numerical simulation are presented in Table 2. In this simulation a number of discrete elements for the rod were tested, including 10, 100, 1,000, and 10,000. It was demonstrated that with 1,000 elements the results of the simulation remained constant.

Parameter	Value
Sound velocity in rods, ft/s	15,700
Rod material modulus of elasticity, MPa	30.5
Column length rods, ft	2,200
Pump speed, spm	12.5
Polished rod stroke, pol	42
Rods diameter, in	0.75
Specific weight of the rod material, lbf /ft^3	495.33
Specific gravity of the fluid, ---	0.82
Production column diameter, in	2.375
Piston diameter, in	1.5
Fluid produced viscosity, cP	10

Table 1. Operational and geometric parameter

Parameter	Value
Number of elements, ---	1,000
Element size, ft	2.2
Number of time steps, ---	100,000
Time step, s	0.00011
Total simulation time, s	11

Table 2. Parameters used for a 2,200 ft long rod column.

Figure 8 depicts the surface dynamometer chart representing the load value on the polished rod according to its position. This allows for the determination of some operating parameters of the system, such as the maximum (PPRL - maximum polished rod load) and minimum (MPRL - minimum polished rod load) loads on the polished bar. In this case, the values obtained were 8,202.9 and 1,611.6 pounds (lb in the figure), respectively. Figure 9 shows the downhole dynamometric chart.

Figure 10 depicts a variation of the downhole dynamometric chart presented in Figure 9, wherein the length of the tubing has been increased from 2,200 ft to 3,200 ft. Upon comparison, it becomes evident that the novel result exhibits a more pronounced elongation and a greater distortion in the calculations during both the ascending and descending movements. According to Gomes (2009), The surface chart is susceptible to distortion from the propagation of the effects generated by the rod column, rendering it an inefficient tool of analysis in certain cases, particularly when the depth of the wells exceeds 1,000 meters.

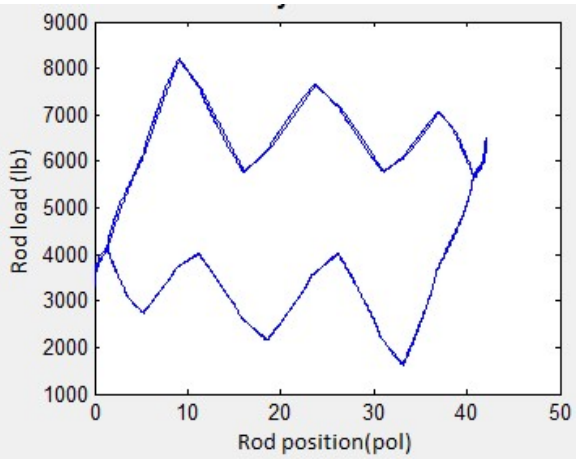

Figure 8. Surface dynamometer chart for a 2,200 ft long rod column.

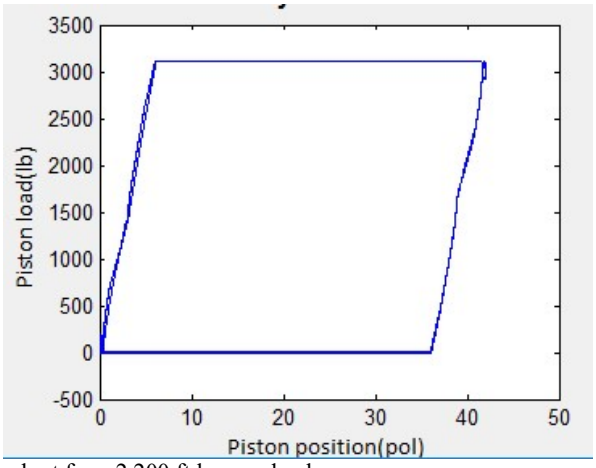

Figure 9. Downhole dynamometer chart for a 2,200 ft long rod column.

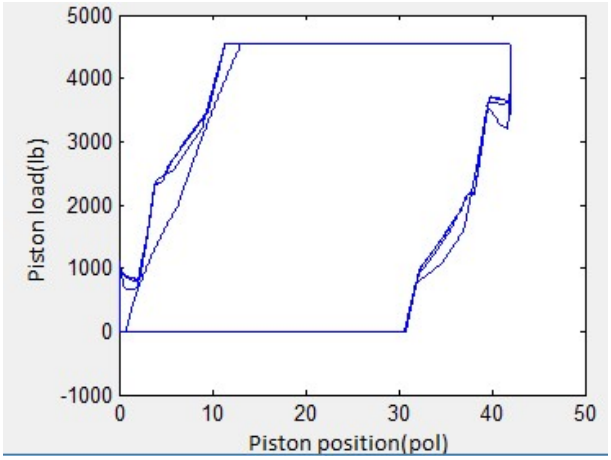

Figure 10. Downhole dynamometer chart for a 3,200 ft long rod column.

6.1 Lea's model (1990)

In this simulation, the same parameters from Tables 1 and 2 were utilized to construct the model within the application. The objective was to ascertain whether the discrepancies would be discernible when a more recent model was employed. The Lea model incorporates a greater number of variables in its calculation of the damping factor, which is not included in the Gibbs (1963) model.

Lea's model (1990) exhibits larger values than the Gibbs model (1963), a result that was anticipated based on the conditions considered by Lea (1990). These differences can be observed in Table 3.

	PPRL, lbs	MPRL, lbs
Gibbs's model (1963)	8,202.9	1,611.6
Lea's model (1990)	8,611.6	1,632.3

Table 3. Results of the cases simulated for a 2,200 ft long rod column.

Figure 11 depicts a downhole dynamometric chart for a 2,200-foot segment of the rod column. Figure 12 depicts the downhole dynamometric chart for a rod column measuring 3,200 ft in length.

The figures illustrate the identical comparison made in the simulation with the Gibbs model. The outcomes are strikingly comparable to those of the preceding model, thereby substantiating the veracity of both models. It should be noted that the Lea model considers the viscosity of the fluid produced and the damping factor, which renders it a more comprehensive model than the Gibbs model.

The simulator additionally furnishes the Courant number for the two models following the simulation process, which is 0.785.

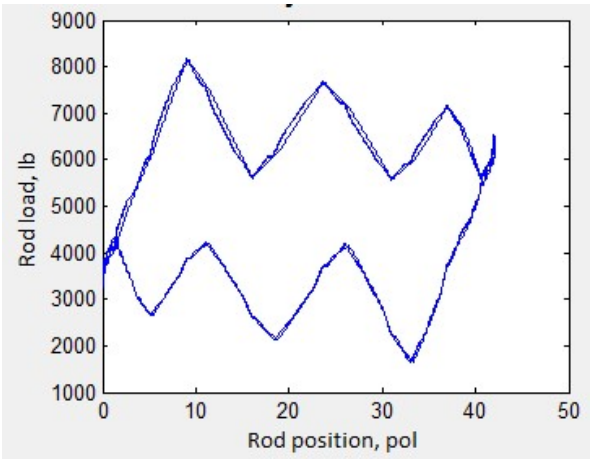

Figure 11. Surface dynamometer chart for a 2,200 ft long rod column.

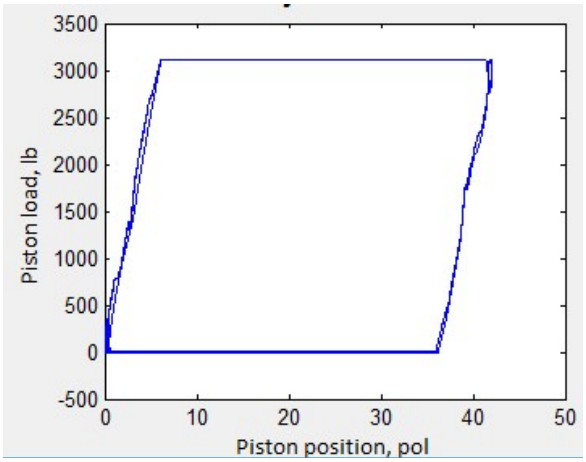

Figure 12. Downhole dynamometer chart for a 2,200 ft long rod column.

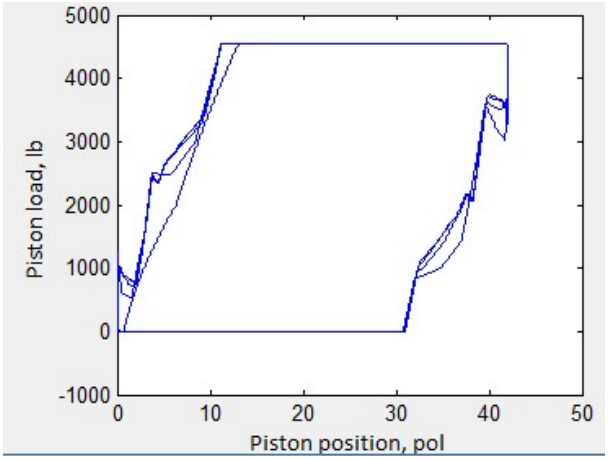

Figure 13. Downhole dynamometer chart for a 3,200 ft long rod column.

7 Final considerations

This work presents the most significant stages of development of the RodSim, an academic simulator. The RodSim can be used for teaching purposes in topics related to sucker rod pumps, or to develop research projects at undergraduate and graduate programs.

The methodology employed was derived from the work of Gibbs (1963) and Lea (1990). In calculating the damping factor, Lea (1990) considers the viscosity of the produced fluid, the piston diameter, the rod diameter, and the diameter of the production column.

It is still considered that the damping factors in the upstroke and downstroke are different, and thus, the results presented in the dynamometric charts are more accurate.

In the RodSim interface, the user defines input parameters, which are then used to generate two dynamometric charts: one for downhole conditions and one for surface conditions.

Nevertheless, several potential enhancements could be implemented, including the effects of rod connections, gas bubbles, sediments, and so forth.

Acknowledgements

Professor Oldrich Joel Romero extends his gratitude to the Fapes – Foundation for Research and Innovation of Espírito Santo for their financial support, as evidenced by Fapes Notice No 6/2021 – Capixaba Researcher Scholarship, TO 356/2022.

References

Bellarby, J (2009) 'Well Completion Design', Jordan Hill, OX: Elsevier (DPS 56).

Costa, RO (2009) 'Curso de Bombeio Mecânico' (in Portuguese), Petrobras.

Doty, DR, Schmidt, Z (1983) 'An improved model for sucker rod pumping', *SPE Journal*, 23(1), 33-41. https://doi.org/10.2118/10249-PA

Gomes, HP (2009) 'Desenvolvimento de um sistema inteligente para a análise de cartas dinamométricas no método de elevação por bombeio mecânico' (in Portuguese). Master's theses, Federal University of Rio Grande do Norte, Natal, RN, Brazil.

Guo, B, Lyons, WC, and Ghalambor, A (2007) 'Petroleum Production Engineering: A Computer-Assisted Approach'. Burlington, MA: Gulf Professional Publishing.

Lea, JF (1990) 'Modeling forces on a bean pump system when pumping highly viscous crude', *SPE Production Engineering*, 6(4), 420-426. https://doi.org/10.2118/20672-PA

Lima, FS, Guedes, LAH, and Silva, DR (2009) 'Detecção de falhas no sistema de Bombeio Mecânico utilizando descritores de Fourier e ferramentas estatísticas' (in Portuguese), *Simpósio Brasileiro de Automação Inteligente*. Aracaju, SE: Petrobras, 2009.

Romero, OJ, Almeida, P (2014) 'Numerical simulation of the sucker-rod pumping system', *Ingeniería e Investigación*, 34(3), 4-11. https://doi.org/10.15446/ing.investig.v34n3.40835

Gibbs, SG (1963) 'Predicting the Behavior of Sucker-Rod Pumping Systems', *Journal of Petroleum Technology*, 15(7), 769-778. https://doi.org/10.2118/588-PA

Rowlan, OL, Mccoy, JN, and Podio, AL (2005) 'Best method to balance torque loadings on a pumping unit gearbox', *Journal of Canadian Petroleum Technology* – JCPT, 44(7): 27-33. https://doi.org/10.2118/05-07-TN3

Schmidt, Z, and Doty, DR (1989) 'System Analysis for Sucker-Rod Pumping', *SPE Production Engineering*, 4(2). https://doi.org/10.2118/15426-PA

Silva, WL, Netoy, DGS, Barreto, MA, Lima, AMN, and Oliveira, A (2014) 'Determining the surface dynamometer card of a pumping system from the torque curve of a three-phase induction motor'. *Anais do XX Congresso Brasileiro de Automática* (In Portuguese), Belo Horizonte, September. 20-24, 2014.

Tákacs, G (2023) 'Sucker-rod pumping manual'. Tulsa, Oklahoma: PennWell Books.

Thomas, JW (1995) 'Numerical partial differential equations: Finite difference methods'. New York, NY: Springer-Verlag.